Journal of Molecular Graphics and Modelling 29 (2010) 221–228

Contents lists available at ScienceDirect

Journal of Molecular Graphics and Modelling

journal homepage: www.elsevier.com/locate/JMGM

Force field design and molecular dynamics simulations of factor-inhibiting HIF-1 and its complex with known inhibitors: Implications for rational inhibitor design

Hwangseo Park[a,*], Sungmin Ko[a], Young Ho Jeon[b,c,**]

[a] Department of Bioscience and Biotechnology, Sejong University, 98 Kunja-Dong, Kwangjin-Ku, Seoul 143-747, Republic of Korea
[b] Division of Magnetic Resonance, Korea Basic Science Institute, 804-1 Yangchung-Ri, Ochang, Chungbuk 363-883, Republic of Korea
[c] Bio-Analytical Science Program, University of Science and Technology, Daejeon 350-333, Republic of Korea

ARTICLE INFO

Article history:
Received 2 February 2010
Received in revised form 23 June 2010
Accepted 24 June 2010
Available online 1 July 2010

Keywords:
Factor-inhibiting HIF-1
Molecular dynamics
Force field development
Inhibitor
Drug design

ABSTRACT

Based on molecular dynamics simulations in aqueous solution, we investigate the dynamic properties of factor-inhibiting HIF-1 (FIH1) and its complexes with the substrate 2-oxoglutarate (2OG) and the two known inhibitors, N-oxalylglycine (NOG) and N-oxalyl-D-phenylalanine (NODP). The results obtained with the newly developed force field parameters for the coordination environment of the active-site ferrous ion show that FIH1 undergoes a significant conformational stabilization with a decrease in motional amplitude upon binding of the substrate or the inhibitors. Two loop structures around the active-site reveal a high flexibility in the resting form of FIH1 with the high *B*-factor values. These high-amplitude motions of the flexible loops are found to be weakened significantly in the presence of the substrate or a weak inhibitor (NOG), and damped out upon binding of a potent and selective inhibitor (NODP) in the active site. A characteristic feature that discriminates the coordination structures of the active-site ferrous ion in complex with 2OG and NOG in solution from those in the X-ray crystal structures lies in the presence of a structural water molecule from bulk solvent at the sixth coordination position, which leads to the formation of a stable octahedral coordination geometry. However, the approach of such a structural water molecule to the active-site ferrous ion is prohibited in the FIH1–NODP complex, which should be attributed to the formation of hydrophobic contacts between the phenyl ring of the inhibitor and the side chains of Tyr102, Leu186, and Trp296 at the entrance of the active site. This indicates that the D-enantiomeric side-chain phenyl group of NODP should play an essential role in potent and selective inhibition of FIH1.

1. Introduction

Hypoxia refers to a local decrease in the cellular oxygen concentration to an abnormal extent. This results from a variety of pathophysiologic components including anemia, ischemic and vascular diseases [1]. Since mammalian cells depend on the molecular oxygen for survival, they should have a proper mechanism to sustain the oxygen concentration at a normal level. In case of human, hypoxia has been known to be responsible for angiogenesis and erythropoiesis which are respectively induced by vascular endothelial growth factor (VEGF) and erythropoietin (EPO) [2–5].

Hypoxia-inducible factor-1 (HIF-1) is a master regulator that controls the transcription of hypoxia-inducible proteins including VEGF and EPO [6,7]. HIF-1 belongs to the basic helix-loop-helix (bHLH) PAS family [8] and acts in a heterodimeric form comprising α and β subunits [9]. HIF-1β is expressed in nucleus in a constitutive fashion whereas the expression of HIF-1α is affected by the cellular oxygen levels. For this reason, the α subunit is responsible for the oxygen-dependent transcriptional activity of HIF-1 [10–13]. HIF-1α contains two regions that are sensitive in particular to the cellular oxygen levels: N-terminal transactivation domain (N-TAD) and C-terminal transactivation domain (C-TAD) [14]. The former resides within the oxygen-dependent degradation (ODD) domain and includes the two conserved proline residues, Pro402 and Pro564 [15]. The hydroxylations at these proline residues lead to the proteasomal destruction due to the resulting interaction with the von Hippel–Lindau (VHL) E3 ubiquitin ligase complex [16]. Prolyl hydroxylase domain-containing protein (PHD), which is also known as Egl nine homolog (EGLN), targets the conserved

* Corresponding author.: Tel.: +82 2 3408 3766; fax: +82 2 3408 4334.
** Corresponding author.
E-mail addresses: hspark@sejong.ac.kr (H. Park), yhjeon@kbsi.re.kr (Y.H. Jeon).

1093-3263/$ – see front matter © 2010 Elsevier Inc. All rights reserved.
doi:10.1016/j.jmgm.2010.06.009

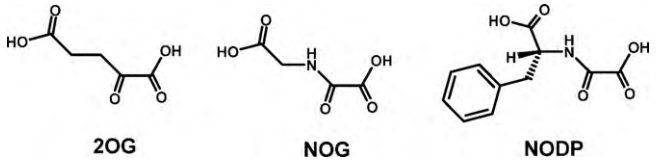

Fig. 1. Molecular structures of 2-oxoglutarate (2OG), N-oxalylglycine (NOG), and N-oxalyl-D-phenylalanine (NODP).

LxxLAP motif in N-TAD with the hydroxylation of the terminal proline residue in the motif [17]. On the other hand, C-TAD includes a conserved asparaginyl residue (Asn803 in human HIF-1α), the hydroxylation of which at C_β atom inhibits the transcriptional activity HIF-1 by blocking the interaction between C-TAD and transcriptional coactivator p300 [18,19].

The hydroxylation state of Asn803 in HIF-1α is regulated by an HIF asparaginyl hydroxylase known as factor-inhibiting HIF-1 (FIH1) [20]. FIH1 is 2-oxoglutarate (2OG)-dependent dioxygenase containing a non-heme ferrous ion at the catalytic center. FIH1 absolutely requires the molecular oxygen for the hydroxylation of Asn803 of HIF-1α, leading to the formation of succinate with the release of CO_2. X-ray crystallographic studies of FIH1 indicated the coordination of the active-site ferrous ion by two histidine (His199 and His279) and one aspartate (Asp201) residues with the remaining coordination sites being occupied by water molecules in the resting form and by molecular oxygen and 2OG during the catalytic reactions [21,22]. Computational studies have also been performed to supplement the experimental findings. Based on the molecular dynamics (MD) simulation studies for FIH1 in complex with various HIF-1α mutants in C-TAD, Linke et al. identified the amino acids of FIH1 that play a crucial role in accommodating Asn803 of HIF-1α [23].

Due to the effective regulation of HIF-1, FIH1 has been considered as a good therapeutic target for anemia and ischemic diseases. The development of small-molecule FIH1 inhibitors has nonetheless lagged behind the biological and structural findings. Only a few substrate-analog inhibitors of FIH1 have been reported so far. In this regard, earlier studies indicated that a cell-permeable 2OG analog such as dimethyl-oxalylglycine (DMOG) could block the asparaginyl hydrolase activity of FIH1 [20,24]. N-oxalylglycine (NOG) is another known FIH1 inhibitor with K_i value of 1.2 mM although it can also inhibit the catalytic activities of most of the enzymes in Fe(II)- and 2OG-dependent dioxygenase superfamily. The lack of selectivity in the inhibition of FIH1 made it unworthy of further development for antianemia drugs. A series of N-oxalyl amino acids have also been shown to be substrate-analog inhibitors of FIH1 with varying inhibitory activities [25]. Among them, some of the D-enantiomers derived from the hydrophobic amino acids such as N-oxalyl-D-phenylalanine (NODP) revealed a high selectivity in the inhibition of FIH1 with K_i value of 83 μM. X-ray crystallographic analyses showed that the substrate-analog inhibitors NOG and NODP would bind in the active site of FIH1 in a similar fashion to the substrate 2OG: 1′-carboxylate and carbonyl group are coordinated to the central ferrous ion with the formation of the hydrogen bonds (HBs) between 5′-carboxylate and Tyr145, Thr196, and Lys214 [22].

In the present study, we examine the dynamic properties of FIH1 in the resting form and in complexes with 2OG, NOG, and NODP whose chemical structures are shown in Fig. 1. For this purpose, molecular dynamics (MD) simulations are carried out using the newly developed force field parameters for active-site ferrous ion and its coordination environment that are unavailable in the standard force field database. These force field parameterizations are performed with the high-level quantum chemical calculations on the ferrous ion clusters modeling the enzymatic active site in the resting form and that complexed with the ligands. During the course of MD simulations of unliganded and liganded forms of FIH1, we aim to address the significant interactions that stabilize the enzyme–ligand complexes in aqueous solution. By comparing the results for bound and unbound forms of FIH1, we also investigate the influence of ligand binding on the dynamic stability of the overall protein structure and the motional amplitudes of protein regions. It will be shown that the solution-phase MD simulations can provide valuable information for designing a new potent inhibitor of FIH1.

2. Computational methods

2.1. Force field design for the active-site ferrous ion complex

MD simulations of FIH1 and its complexes with ligands were carried out using the AMBER program (version 7) with the force field parameters reported by Cornell and coworkers [26]. The bonded approach [27] was adopted to represent a metal ion with placing the explicit bonds between the ferrous ion and its ligand atoms because the other non-bonded counterparts have been known to be sensitive to the employed electrostatic model, leading to the disruption of the coordination geometry [28,29]. To derive the associated force field parameters that are unavailable in the standard force field database, we followed the procedure suggested by Fox and Kollman [30] to be consistent with the standard AMBER force field [26]. The equilibrium bond lengths and angles involving the active-site ferrous ion were taken from the optimized structures of the ferrous ion chelated with the 2-oxo-carboxylate group of the substrate and the inhibitors. These geometry optimizations were carried out with density functional calculations at B3LYP/6-31G* level of theory using Gaussian03 suite of program. The starting coordinates were prepared by extracting the atomic coordinates from the X-ray crystal structures of FIH1 in complexes with 2OG, NOG, and NODP (PDB entries: 1H2L, 1H2K, and 1YCI, respectively) [21,25]. Due to the lack of the X-ray crystal structure, the coordinates of apoenzyme were obtained by removing the substrate 2OG in the FIH1–2OG complex. For the force constant parameters involving the ferrous ion, we used the values in the earlier Giammona's work [31]. Using the energy-minimized structures, atomic partial charges were calculated at RHF/6-31G* level of theory with the RESP method [32] to be consistent with the standard AMBER force field. The geometries of 2OG, NOG, and NODP were also optimized to compute their atomic charges with the RESP method at RHF/6-31G* level of theory. Missing force field parameters for the ligands were estimated from those for similar chemical species in the AMBER force field database.

2.2. MD simulations

After removing the solvent molecules in the crystal structures of FIH1 in complex with the substrate and the inhibitors, hydrogen atoms were added to the protein atoms. A special attention was paid to assign the protonation states of the ionizable Asp, Glu, His, and Lys residues. The side chains of Asp and Glu residues were assumed to be neutral if one of their carboxylate oxygens pointed toward an HB accepting group including the backbone aminocarbonyl oxygen at a distance within 3.5 Å, a generally accepted distance limit for an HB with moderate strength [33]. Similarly, the lysine side chains were protonated unless the NZ atom was in proximity of an HB donating group. The same procedure was applied to determine the protonation states of ND and NE atoms in His residues. Actually, the ionizable residues are very unlikely to exist in the unionized form in protein structure because of the high acidity and basicity. Indeed, only two (Asp134 and Glu141)

of 16 Asp and 28 Glu residues were assumed to be protonated with no neutral Lys residue in FIH1. This is because their side-chain carboxylate groups appear to donate a hydrogen bond to a backbone aminocarbonyl carbon in the X-ray crystal structure with the associated interatomic distances of 2.82 and 3.46 Å, respectively.

After adding nine sodium ions for charge neutralization, the all-atom models for the unliganded and liganded FIH1 were immersed in rectangular boxes containing about 15,000 TIP3P [34] water molecules. After 200 cycles of energy minimization to remove the bad steric contacts, we equilibrated the systems beginning with 20 ps equilibration dynamics of the solvent molecules at 300 K. The next step involved the equilibration of the solute with a fixed configuration of solvent molecules consecutively at 10, 50, 100, 150, 200, 250, and 300 K for 10 ps at each temperature. Then, the equilibration dynamics of the entire system was performed at 300 K for 100 ps.

Following the equilibration procedure, 5.1 ns MD simulations were carried out with periodic boundary conditions in the NPT ensemble. The temperature and pressure were kept at 300 K and 1 atm using Berendsen temperature coupling [35] and isotropic molecule-based scaling, respectively. The SHAKE algorithm [36], with a tolerance of 10^{-6}, was applied to fix all bond lengths involving the hydrogen atom. We used a time step of 1.5 fs and a non-bond-interaction cutoff radius of 12 Å; the trajectory was sampled every 0.3 ps (200-step intervals) for analysis. The 17,000 conformations sampled during the MD simulation of each enzyme–ligand complex were clustered using the PTRAJ program in AMBER 7 [37] accoriding to the RMSD of atomic coordinates. The trajectory snapshot closest to the centroid of the cluster with the highest population was then selected as the representative structure of each enzyme–ligand complex.

3. Results and discussion

3.1. Force field design for the active-site ferrous ion cluster

To extend the AMBER force field parameter space so as to be able to model the ferrous ion cluster in the active site of FIH1, we followed the procedure suggested by Fox and Kollman [30]. This approach starts with the geometry optimizations of the relevant model systems for the active-site ferrous ion cluster and its complexes with the substrate (2OG) and the inhibitors (NOG and NODP). In these model systems, methyl imidazole and acetate ion were used to respectively represent the two histidine (His199 and His279) and one aspartate (Asp201) residues coordinated to the central ferrous ion. Fig. 2 displays the structures of the model FIH1–ligand complexes optimized at B3LYP/6-31G* level of theory. Consistent with the original X-ray crystal structures, all of the ferrous ion clusters reveal a distorted square pyramidal geometry with the axial position being occupied by the NE2 atom of His279. It is also a common structural feature among the three complexes that 1′-carboxylate oxygen (O2) and the carbonyl oxygen (O1) of the ligands chelate the ferrous ion at the two equatorial positions. In the optimized structure of the model FIH1–NODP complex, it is noteworthy that the side-chain phenyl ring is directed to the vacant axial position, which would have the effect of preventing the sixth ligand from approaching the central ferrous ion. Interatomic distances associated with the ferrous ion also compare reasonably well with those in the crystal structures with the differences of 0.08, 0.10, and 0.17 Å on average for FIH1–2OG, FIH1–NOG, and FIH1–NODP complexes, respectively. The structures shown in Fig. 2 were used as the input structures in the subsequent atomic charge calculations with the RESP method. Due to the lack of the X-ray crystal structure for the ligand-free form of FIH1, the active-site ferrous ion cluster for apoenzyme was obtained

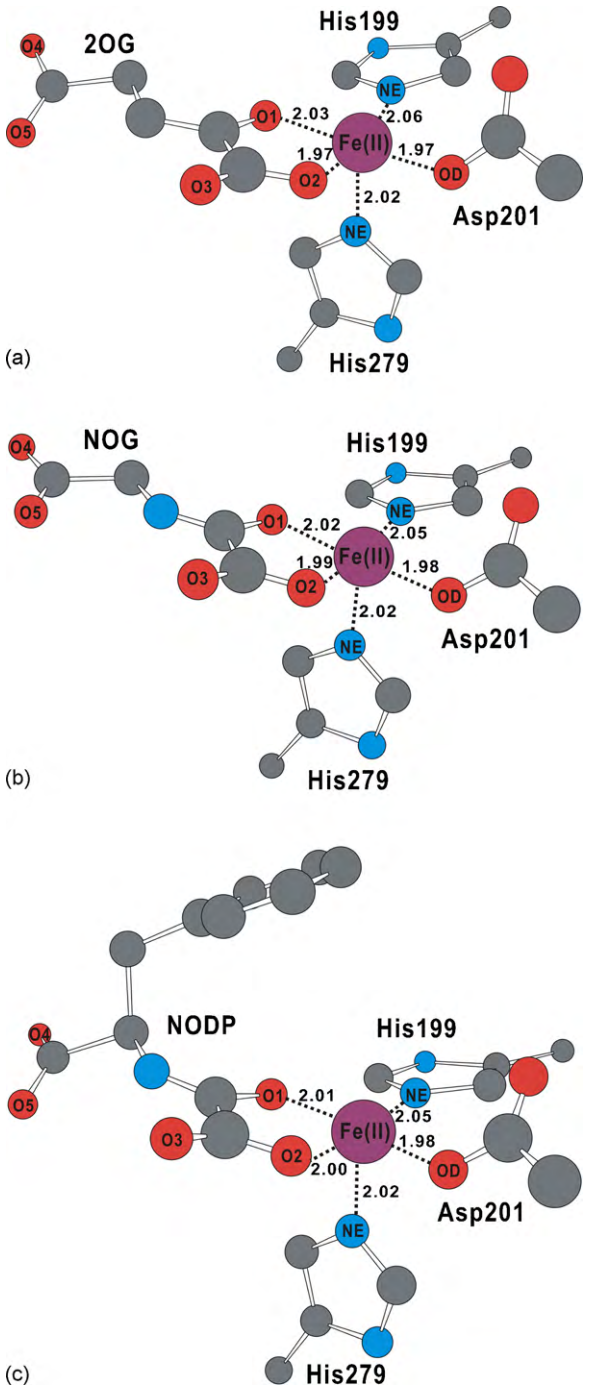

Fig. 2. B3LYP/6-31G* optimized structures of the central ferrous ion cluster in complex with (a) 2OG, (b) NOG, and (c) NODP.

by removing the substrate 2OG in the optimized FIH1–2OG complex.

Table 1 lists the RESP atomic charges of the central ferrous ion and its ligand atoms calculated with the optimized structures shown in Fig. 2. We note that the atomic charge of the ferrous ion decreases from +2.000e in its free state to +1.346e on average upon the complexation with the substrate and the inhibitors. On the other hand, the atomic charges of the ligand atoms become less negative by 0.101–0.128e for the NE atoms of His199 and His279, by 0.176–0.234e for the carboxylate oxygen of Asp201 and the ligands, and by 0.123e on average for the carbonyl oxygen (O1) of the substrate and the inhibitors when compared to those in the absence of the ferrous ion. These changes reflect the redistribution of charges

Table 1
RESP charges (in e) of the ferrous ion and its ligand atoms in the model systems for FIH1 in complex with the substrate and the inhibitors, in comparison with those before the formation of a metal complex. See Fig. 2 for the identification of atoms.

Atoms	RESP charges			
	In free state	FIH1–2OG	FIH1–NOG	FIH1–NODP
Fe^{2+}	+2.000	+1.375	+1.342	+1.321
His199 NE	−0.472	−0.350	−0.371	−0.363
Asp201 OD	−0.761	−0.547	−0.527	−0.549
His279 NE	−0.472	−0.350	−0.344	−0.352
O1	−0.599	−0.476	−0.470	−0.481
O2	−0.778	−0.595	−0.602	−0.586

between the ferrous ion and its ligand atoms upon the formation of a transition–metal complex, exemplifying that the 'M^{n+}' model should be inadequate for describing the active-site metal ion clusters of metalloenzymes [38]. We used the newly obtained RESP atomic charges listed in Table 1 in the subsequent MD simulations of FIH1 in complex with the substrate and the inhibitors.

3.2. MD simulations

Fig. 3 compares the time evolutions of root-mean-square deviation from the initial structure for all backbone C_α atoms ($RMSD_{init}$) of FIH1 in the resting form and those in the FIH1–2OG, FIH1–NOG, and FIH1–NODP complexes. We note that the $RMSD_{init}$ values of FIH1 remain within 2.5 Å for 5.1 ns of simulation time with a convergent behavior in both bound and unbound simulations. This indicates that the conformation of FIH1 would be maintained stable irrespective of ligand binding, which is consistent with the stability of the overall protein structure toward ligand binding as revealed by X-ray crystallographic data [21]. It is also noteworthy that the $RMSD_{init}$ values of ligand-bound FIH1 remain lower than those for apoenzyme during the entire course of simulation, indicating that ligand binding in the active site would lead to a further conformational stabilization of FIH1. Judging from the lower $RMSD_{init}$ values of the inhibitor bound forms of FIH1 than those of apoenzyme and FIH1–substrate complex in the later part of simulation, it seems that the effective FIH1 inhibitors should be able to stabilize the conformational motion of FIH1 upon binding in the active site. The protein conformation appears to be most stabilized in FIH1–NODP complex: the $RMSD_{init}$ values of FIH1–NODP complex are maintained around 1.5 Å for the most of simulation time with a convergent behavior whereas those of FIH1–2OG and FIH1–NOG complexes remain between 1.5 and 2.0 Å during the entire course of simulation. Such a dynamic stability of FIH1–NODP complex is consistent with the potent and selective inhibition of FIH1 by NODP, and indicates the existence of some peculiar interactions between FIH1 and NODP that lack in the other FIH1–ligand complexes.

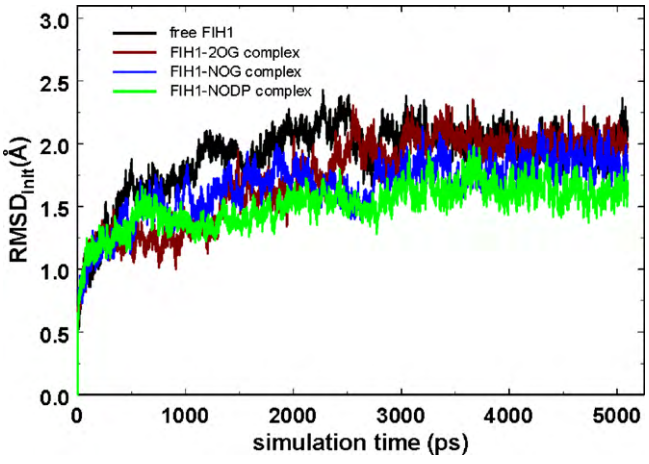

Fig. 3. Time dependences of root-mean-square deviations of backbone C_α atoms from the initial structures ($RMSD_{init}$) for FIH1 in the resting form, FIH1–2OG, FIH1–NOG, and FIH1–NODP complexes.

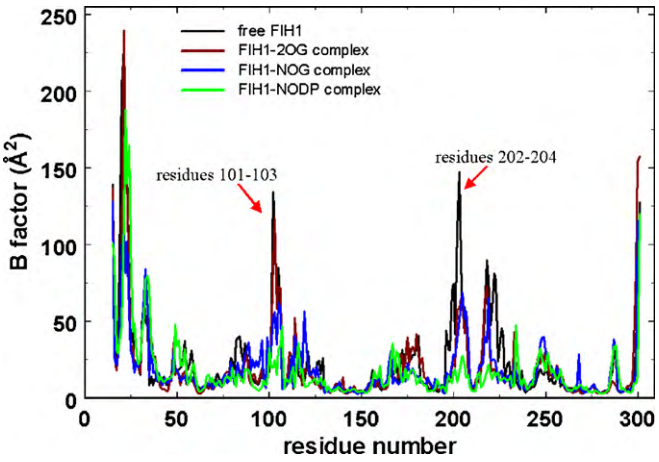

Fig. 4. *B*-factors of C_α atoms for FIH1 in the resting form, FIH1–2OG, FIH1–NOG, and FIH1–NODP complexes. Each *B*-factor value is averaged over 4.6 ns time frame from 0.5 to 5.1 ns.

To examine the change in dynamic flexibilities of the different regions of protein structure due to ligand binding, *B*-factor of the C_α atom for residue i (B_i) was calculated for each residue in both unliganded and liganded forms of FIH1 using the following relationship:

$$B_i = \frac{8}{3}\pi^2\langle\Delta r_i\rangle^2 \quad (1)$$

where $\langle\Delta r_i\rangle$ is RMS atomic fluctuation of the C_α atom of residue i. Although the $\langle\Delta r_i\rangle^2$ values for C_α atoms can be employed to estimate the motional amplitude of a protein backbone in themselves, we used *B*-factor values instead because they could show the differences between the residues of FIH1 in a more distinct manner. As shown in Fig. 4, the overall B_i values of FIH1 in the resting form appear to be very different from those of the FIH1–substrate and FIH1–inhibitor complexes, which implies that the ligand binding has a significant effect on the conformational flexibility FIH1 in aqueous solution. In this regard, we note that several residues undergo a substantical decrease in B_i values in the presence of the substrate 2OG and the inhibitors. Aside from the N- and C-terminal regions, the B_i values for the unliganded FIH1 show two major peaks in the regions of residues 101–103 and 202–204. As can be seen in Fig. 5, these two regions correspond to the loop structures that reside in the vicinity of the active site. Therefore, it can be argued that the high-amplitude motions of the flexible loops should be responsible for a broad substrate specificity of FIH1 for a variety of C-TAD polypeptides. Although the first major peak is also observed in the presence of the substrate 2OG, it is lowered to a significant extent in the FIH1–NOG and FIH1–NODP complexes. This indicates that an effective FIH1 inhibitor should be able to reduce the motional amplitude of the loop structure including residues 101–103. The second major peak appears to be lowered significantly only in the presence of 2OG and NOG, suggesting that the motions of the highly flexible residues are restricted upon binding of the ligands in the active site. The binding of NODP seems to have an effect of damping out the high-amplitude motion of the flexible loop including residues 202–204, which can be inferred from a dramatic decrease in the calculated B_i values of Glu202, Gln203, and Gln204 from 112.7 to 22.4 $Å^2$ on average. Because the malleability of the loop structures around the active site has been shown to be an important factor in the catalytic action of the enzymes with

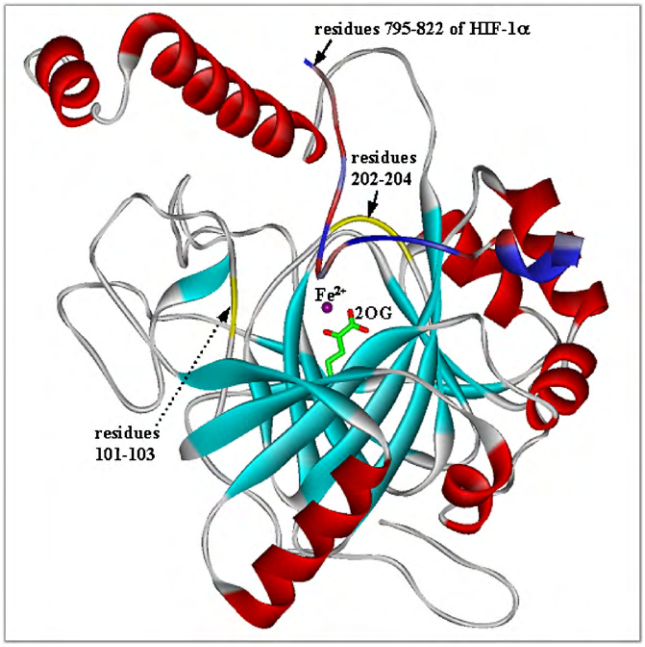

Fig. 5. X-ray crystal structure of FIH1 in complex with HIF-1α and the substrate 2OG. Indicated are the parts of the flexible loops that exhibit a large change in motional amplitude upon binding of the substrate and the inhibitors.

broad substrate specificity [39–41], the high inhibitory activity and selectivity of NODP against FIH1 may be related with its capability to immobilize the two flexible loops that resides in the vicinity of the active site. A significant decrease in B_i values is also observed in the FIH1–NODP complex for the residues 218–223 that belong to a β-sheet that resides distant from the active site.

We now turn to addressing the structural features relevant to the stabilization of the substrate and the inhibitors in the active site of FIH1. Shown in Fig. 6 is the representative MD trajectory snapshot of FIH1–2OG complex. We note that the active-site ferrous ion reveals an octahedral coordination with one of the axial positions being occupied by a solvent molecule that comes from bulk solvent. This sixth coordination bond seems to be dynamically stable because as can be seen in Fig. 7, the interatomic distance between the water oxygen and the central ferrous ion remains within 2.5 Å during the entire course of simulation. Judging from a close proximity of an additional water molecule bridging the water ligand and the side-chain carboxylate group of Asp201 through the HBs, the second water molecule is expected to play a role of maintaining the coordination bond between the ferrous ion and the water ligand. In contrast to the results of MD simulations in aqueous solution, no water molecule was found within the distance of 3.9 Å from the central ferrous ion in the X-ray crystal structures, which indicates the vacancy of the sixth coordination position. Because water molecule is basically a weak ligand for a transition metal ion, its coordination to the ferrous ion seems to be ruptured under the crystallization conditions.

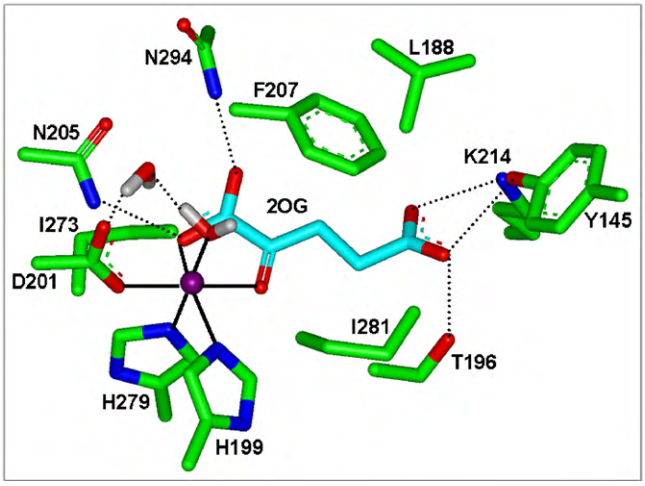

Fig. 6. Representative MD trajectory snapshot for FIH1 in complex with the substrate 2OG. Solid and dotted lines indicate a coordination bond to the ferrous ion and a hydrogen bond, respectively.

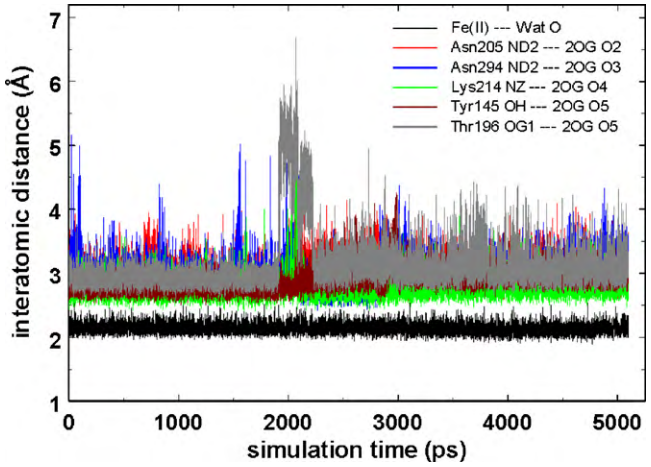

Fig. 7. Time evolutions of the interatomic distances associated with the water coordination to the ferrous ion and the hydrogen bond interactions of 2OG in the active site of FIH1. See Fig. 2 for the identification of 2OG atoms.

The substrate carboxylate oxygens adjacent to the carbonyl group receive the HBs from the side-chain amide groups of Asn205 and Asn294, which seems to have an effect of positioning the ligand atoms in the carboxylate and carbonyl groups near the ferrous ion. This hypothesis may be supported by the dynamic stabilities of the two HBs as shown in Fig. 7: the former and the latter HBs are maintained for 97% and 95% of simulation time, respectively, if the donor–acceptor distance of 3.5 Å is used as the HB-defining distance as suggested by Jeffrey [33]. The other carboxylate group of 2OG also forms the HBs with the side chains of Tyr145, Thr196, and Lys214 at the bottom of the active site. These three HBs appear to be dynamically less stable than those involving the other carboxylate group adjacent to the carbonyl moiety: the HBs donated from the side chains of Tyr145, Thr196, and Lys214 are maintained for 89%, 82%, and 93% of simulation time, respectively. It is interesting to note that the order of the dynamic stabilities of HBs is consistent with that of pK_a values of the side chains of Tyr, Thr, and protonated Lys residues. Besides a direct coordination to the ferrous ion and the multiple HBs, the hydrophobic interactions of 2OG with the side chains of Leu188, Phe207, Ile273, and Ile281 are observed and also likely to be involved in the stabilization of the substrate in the active site. On the basis of these structural features, it can be argued that 2OG binds in the active site of FIH1 through the simultaneous establishment of the multiple HBs and hydrophobic interactions in addition to the chelation of the ferrous ion.

Fig. 8 shows the representative MD trajectory snapshot of FIH1 in complex with the inhibitor NOG. As in the FIH1–2OG complex, a water molecule from bulk solvent occupies the vacant axial position to form an octahedral coordination around the central ferrous ion. As can be inferred from the dynamic stabilities of the coordination distance shown in Fig. 9, the water coordination to the central ferrous ion appears to be stable despite the lack of an additional water molecule positioning the water ligand near the ferrous ion. It is a

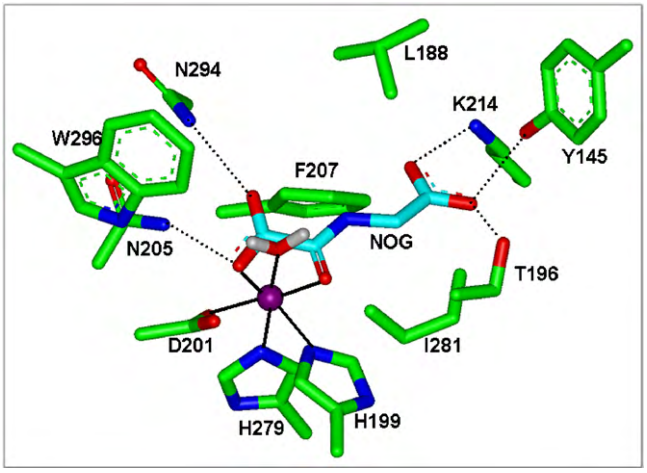

Fig. 8. Representative MD trajectory snapshot for FIH1 in complex with the inhibitor NOG. Solid and dotted lines indicate a coordination bond to the ferrous ion and a hydrogen bond, respectively.

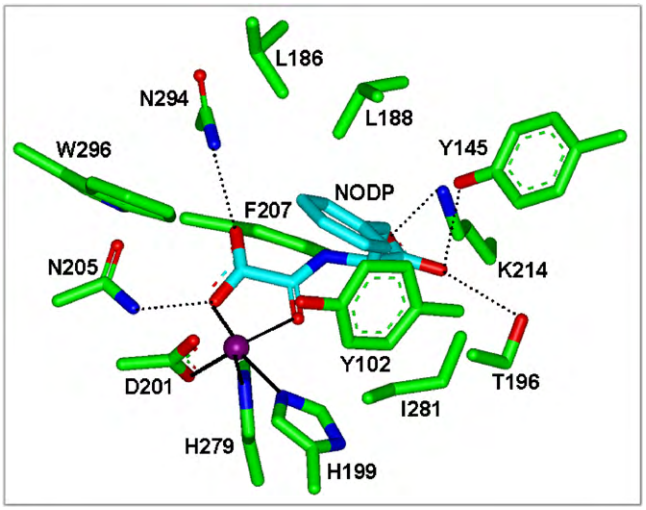

Fig. 10. Representative MD trajectory snapshot for FIH1 in complex with the inhibitor NODP. Solid and dotted lines indicate a coordination bond to the ferrous ion and a hydrogen bond, respectively.

common structural feature that the carboxylate moiety adjacent to the carbonyl group receives two HBs from the side chains of Asn205 and Asn294, the dynamic stabilities of which are also similar to those in the FIH1–2OG complex. The other carboxylate group is stabilized by three HBs donated from the side chains of Tyr145, Thr196, and Lys214. As can be seen in Fig. 9, these HBs seems to be dynamically more stable than the corresponding HBs in the FIH1–2OG complex: the HBs donated from Tyr145, Thr196, and Lys214 are maintained for more than 99% of simulation time in the FIH1–NOG complex as compared to 88% on average in the FIH1–2OG complex. Hydrophobic interactions in the FIH1–NOG complex appear to be established also in a stronger form than those in the FIH1–2OG complex, because an additional hydrophobic residue (Trp296) resides in a close proximity to the inhibitor as well as the side chains of Leu188, Phe207, Ile273, and Ile281. Thus, the interactions with the active-site residues in the FIH1–NOG complex seem to be stronger than that in the FIH1–2OG complex, which is consistent with the fact that NOG is an effective substrate-analog inhibitor of FIH1.

As can be seen in Fig. 10, the HBs in the FIH1–NODP complex are established in a similar fashion to those in the FIH1–2OG and FIH1–NOG complexes. These hydrogen bonds appear to be dynamically stable and observable in most of MD trajectories (Fig. 11): they are maintained for at least 94% of simulation time. This indicates that the extent of contribution from the HBs to the stabilization of the ligand would be similar in the three protein–ligand complexes. One of the characteristic features that discriminate the structure of FIH1–NODP complex from those of FIH1–2OG and FIH1–NOG complexes lies in that the sixth coordination site of the ferrous ion remains vacant: no water molecule is found within 4 Å of the central ferrous ion during the entire course of simulation. This result implies that the binding of NODP to FIH1 would prevent the diffusive intrusion of solvent molecules into the active site. Therefore, the approach of the substrate dioxygen to the central ferrous ion seems also to be limited in the presence of NODP because of its larger molecular volume than the water molecule. Because molecular oxygen is also required during the catalytic cycle of FIH1 as well as the substrates, the difficulty in its binding to the ferrous ion in FIH1–NODP complex can be invoked to explain the high inhibitory activity of NODP.

The hydrophobic interactions in the FIH1–NODP complex appear to be established in a stronger form than those in the FIH1–2OG and FIH1–NOG complexes. This is not surprising for the presence of the phenyl ring in the molecular structure of NODP. Besides the hydrophobic residues that were also found at the interface of the FIH1–2OG complex (Leu188, Phe207, Ile273, and Ile281),

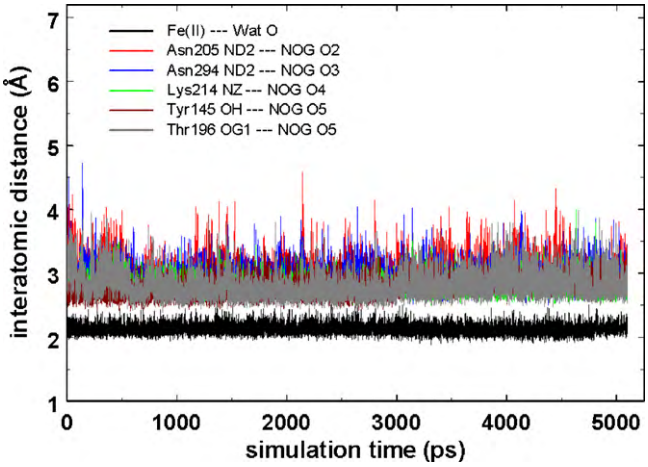

Fig. 9. Time evolutions of the interatomic distances associated with the water coordination to the ferrous ion and the hydrogen bond interactions of NOG in the active site of FIH1. See Fig. 2 for the identification of NOG atoms.

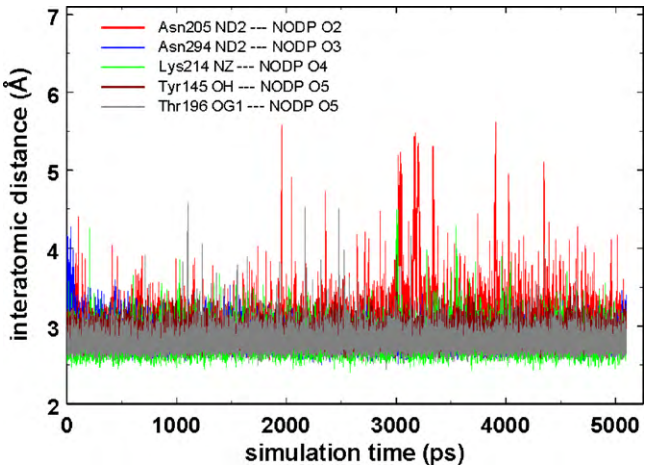

Fig. 11. Time evolutions of the interatomic distances associated with the hydrogen bond interactions of NODP in the active site of FIH1. See Fig. 2 for the identification of NODP atoms.

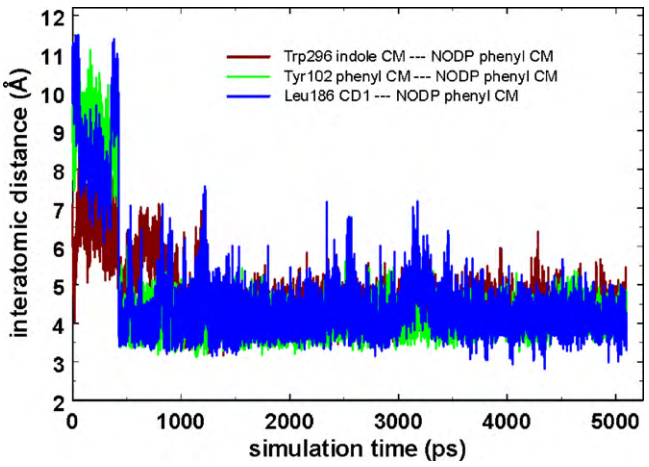

Fig. 12. Time evolutions of the interatomic distances associated with the hydrophobic interactions of NODP in the active site of FIH1. CM indicates the center of mass.

three additional residues including Tyr102, Leu186, and Trp296 are involved in the stabilization of the phenyl ring of NODP in the active site. As shown in Fig. 12, the hydrophobic interactions between the inhibitor phenyl ring and the side chains of Tyr102, Leu186, and Trp296 are established in the early stage of simulation and maintained for the most of simulation time, which indicates that such hydrophobic interactions should be a significant binding force stabilizing NODP in the active site of FIH1. These hydrophobic interactions seem to be formed in the present MD simulations as a consequence of structural relaxation of the enzyme-inhibitor complex in aqueous solution because they were not observed in the original crystal structure. Judging from a close proximity of Tyr102 to NODP, the aforementioned decrease in the motional amplitude of the flexible residues 101–103 in the presence of NODP may be attributed to the hydrophobic interaction of Tyr102 with the inhibitor phenyl ring. Besides the role in stabilizing the inhibitor, the hydrophobic cluster comprising the inhibitor phenyl group and the side chains of Tyr102, Leu186, and Trp296 seems to play a role of covering the active site, which has the effect of preventing the substrate from approaching the sixth coordination position of the central ferrous iron.

It is known that D-enantiomer of N-oxalyl-phenylalanine has the higher inhibitory activity than the *L* enantiomer [25]. This can be understood by reminding the importance of the terminal carboxylate and phenyl groups for the stabilization of the D-enantiomer in the active site: the former establishes the multiple HBs at the bottom of the active site while the latter is stabilized through van der Waals contacts with the hydrophobic residues. It is therefore apparent that the structural transition from D- to L-enantiomers by the change of the positions of the two moieties would have the effect of weakening the HB and hydrophobic interactions between the inhibitor and the active-site residues. Thus, the structural features derived from the present MD simulations are consistent with the enantiomeric preference of the N-oxalyl-phenylalanine in the inhibition of FIH1.

4. Conclusions

We have investigated the dynamic properties of FIH1 in the resting form and its complexes with the substrate 2OG and the two known inhibitors (NOG and NODP) in aqueous solution by means of MD simulations with the newly developed force field parameters for the central ferrous ion clusters. The results indicate that binding of the substrate and the inhibitors would cause a conformational stabilization of FIH1 with a decrease in motional amplitude. Two loop structures around the active site are found to be most flexible in the resting form of FIH1. Such a high-amplitude motion of the flexible loops is found to be damped out upon binding of NODP in the active site. In the FIH1–2OG and FIH1–NOG complexes, a structural water molecule from bulk solvent occupies the sixth coordination position of the central ferrous ion to form a dynamically stable octahedral coordination. However, such a structural water molecule is not found around the ferrous ion in the FIH1–NODP complex. The prevention of the approach of an additional ligand to the sixth coordination position should be attributed to the formation of hydrophobic interactions between the phenyl ring of the inhibitor and the side chains of Tyr102, Leu186, and Trp296 at the entrance of the active site. This indicates that the D-enantiomeric side-chain phenyl group of NODP should be responsible for its potent and selective inhibition of FIH1. The structural and dynamical features of FIH1 derived from MD simulations can thus serve as valuable information for designing new FIH1 inhibitors.

Acknowledgement

This work was supported by High Field NMR Research Program (to Y.H.J.) of Korea Basic Science Institute.

References

[1] G.L. Semenza, Transcriptional regulation by hypoxia-inducible factor 1 molecular mechanisms of oxygen homeostasis, Trends Cardiovas. Med. 6 (1996) 151–157.
[2] M. Klagsbrun, S. Soker, VEGF/VPF: the angiogenesis factor found, Curr. Biol. 3 (1993) 699–702.
[3] P.J. Ratcliffe, Molecular biology of erythropoietin, Kidney Int. 44 (1993) 887–904.
[4] H.F. Bunn, R.O. Poyton, Oxygen sensing and molecular adaptation to hypoxia, Physiol. Rev. 76 (1996) 839–885.
[5] K. Guillemin, M.A. Krasnow, The hypoxic response: huffing and HIFing, Cell 89 (1997) 9–12.
[6] G.L. Semenza, G.L. Wang, A nuclear factor induced by hypoxia via de novo protein synthesis binds to the human erythropoietin gene enhancer at a site required for transcriptional activation, Mol. Cell. Biol. 12 (1992) 5447–5454.
[7] Z.K. Otrock, H.A. Hatoum, A.H. Awada, R.S. Ishak, A.I. Shamseddine, Hypoxia-inducible factor in cancer angiogenesis: structure, regulation and clinical perspectives, Crit. Rev. Oncol. Hemat. 70 (2009) 93–102.
[8] G.L. Wang, B.H. Jiang, E.A. Rue, G.L. Semenza, Hypoxia-inducible factor 1 is a basic-helix-loop-helix-PAS heterodimer regulated by cellular O_2 tension, Proc. Natl. Acad. Sci. U.S.A. 92 (1995) 5510–5514.
[9] G.L. Wang, G.L. Semenza, Purification and characterization of hypoxia-inducible factor 1, J. Biol. Chem. 270 (1995) 1230–1237.
[10] M. Ema, K. Hirota, J. Minura, H. Abe, J. Yodoi, K. Sogawa, L. Poellinger, Y. Fujii-Kuriyama, Molecular mechanisms of transcription activation by HLF and HIF1alpha in response to hypoxia: their stabilization and redox signal-induced interaction with CBP/p300, EMBO J. 18 (1999) 1905–1914.
[11] P.J. Kallio, K. Okamoto, S. O'Brien, P. Carrero, Y. Makino, H. Tanaka, L. Poellinger, Signal transduction in hypoxic cells: inducible nuclear translocation and recruitment of the CBP/p300 coactivator by the hypoxia-inducible factor-1α, EMBO J. 17 (1998) 6573–6586.
[12] C.W. Pugh, J.F. O'Rourke, M. Nagao, J.M. Gleadle, P.J. Ratcliffe, Activation of hypoxia-inducible factor-1; definition of regulatory domains within the alpha subunit, J. Biol. Chem. 272 (1997) 11205–11214.
[13] L.E. Huang, Z. Arany, D.M. Livingston, H.F. Bunn, Activation of hypoxia-inducible transcription factor depends primarily upon redox-sensitive stabilization of its alpha subunit, J. Biol. Chem. 271 (1996) 32253–32259.
[14] B.-H. Jiang, J.Z. Zheng, S.W. Leung, R. Roe, G.L. Semenza, Transactivation and inhibitory domains of hypoxia-inducible factor 1 alpha, J. Biol. Chem. 272 (1997) 19253–19260.
[15] L.E. Huang, J. Gu, M. Schau, H.F. Bunn, Regulation of hypoxia-inducible factor 1α is mediated by an oxygen-dependent domain via the ubiquitin-proteasome pathway, Proc. Natl. Acad. Sci. U.S.A. 95 (1998) 7987–7992.
[16] P.H. Maxwell, M.S. Wiesener, G.-W. Chang, S.C. Clifford, E.C. Vaux, M.E. Cockman, C.C. Wykoff, C.W. Pugh, E.R. Maher, P.J. Ratcliffe, The tumour suppressor protein VHL targets hypoxia-inducible factors for oxygen-dependent proteolysis, Nature 399 (1999) 271–275.
[17] K.K.W. To, L.E. Huang, Suppression of hypoxia-inducible factor 1α (HIF-1α) transcriptional activity by the HIF prolyl hydroxylase EGLN1, J. Biol. Chem. 280 (2005) 38102–38107.
[18] D. Lando, D.J. Peet, D.A. Whelan, J.J. Gorman, M.L. Whitelaw, Asparagine hydroxylation of the HIF transactivation domain: a hypoxic switch, Science 295 (2002) 858–861.

[19] K. Hirota, G.L. Semenza, Regulation of hypoxia-inducible factor 1 by prolyl and asparaginyl hydroxylases, Biochem. Biophys. Res. Commun. 338 (2005) 610–616.
[20] S.E. Wilkins, J. Hyvärinen, J. Chicher, J.J. Gorman, D.J. Peet, R.L. Bilton, P. Koivunen, Differences in hydroxylation and binding of Notch and HIF-1α demonstrate substrate selectivity for factor inhibiting HIF-1 (FIH-1), Int. J. Biochem. Cell Biol. 41 (2009) 1563–1571.
[21] J.M. Elkins, K.S. Hewitson, L.A. McNeill, J.F. Seibel, I. Schlemminger, C.W. Pugh, P.J. Ratcliffe, C.J. Schofield, Structure of factor-inhibiting hypoxia-inducible factor (HIF) reveals mechanism of oxidative modification of HIF-1, J. Biol. Chem. 278 (2003) 1802–1806.
[22] C.E. Dann, R.K. Bruick, J. Deisenhofer, Structure of factor-inhibiting hypoxia-inducible factor 1: an asparaginyl hydroxylase involved in the hypoxic response pathway, Proc. Natl. Acad. Sci. U.S.A. 99 (2002) 15351–15356.
[23] S. Linke, C. Stojkoski, R.J. Kewley, G.W. Booker, M.L. Whitelaw, D.J. Peet, Substrate requirements of the oxygen-sensing asparaginyl hydroxylase factor-inhibiting hypoxia-inducible factor, J. Biol. Chem. 279 (2004) 14391–14397.
[24] M. Milkiewicz, C.W. Pugh, S. Egginton, Inhibition of endogenous HIF inactivation induces angiogenesis in ischaemic skeletal muscles of mice, J. Physiol. 560 (2004) 21–26.
[25] M.A. McDonough, L.A. McNeill, M. Tilliet, C.A. Papamicael, Q.-Y. Chen, B. Banerji, K.S. Hewitson, C.J. Schofield, Selective inhibition of factor inhibiting hypoxia-inducible factor, J. Am. Chem. Soc. 127 (2005) 7680–7681.
[26] W.D. Cornell, P. Cieplak, C.I. Bayly, I.R. Gould, K.M. Merz Jr., D.M. Ferguson, D.C. Spellmeyer, T. Fox, J.W. Caldwell, P.A. Kollman, A second-generation force field for the simulation of proteins, nucleic acids, and organic molecules, J. Am. Chem. Soc. 117 (1995) 5179–5197.
[27] S.C. Hoops, K.W. Anderson, K.M. Merz Jr., Force field design for metalloproteins, J. Am. Chem. Soc. 113 (1991) 8262–8270.
[28] R.H. Stote, M. Karplus, Zinc binding in proteins and solution: a simple but accurate nonbonded representation, Proteins: Struct. Funct. Genet. 23 (1995) 12–31.
[29] S. Toba, G. Colombo, K.M. Merz Jr., Solvent dynamics and mechanism of proton transfer in human carbonic anhydrase II, J. Am. Chem. Soc. 121 (1999) 2290–2302.
[30] T. Fox, P.A. Kollman, Application of the RESP methodology in the parameterization of organic solvents, J. Phys. Chem. B 102 (1998) 8070–8079.
[31] D.A. Giammona, Ph.D. Thesis, University of California, Davis, 1984.
[32] C.I. Bayly, P. Cieplak, W.D. Cornell, P.A. Kollman, A well-behaved electrostatic potential based method using charge restraints for deriving atomic charges: the RESP model, J. Phys. Chem. 97 (1993) 10269–10280.
[33] G.A. Jeffrey, An Introduction to Hydrogen Bonding, Oxford University Press, Oxford (1997).
[34] W.L. Jorgensen, J. Chandrasekhar, J.D. Madura, R.W. Impey, M.L. Klein, Comparison of simple potential functions for simulating liquid water, J. Chem. Phys. 79 (1983) 926–935.
[35] H.J.C. Berendsen, J.P.M. Postma, W.F. van Gunsteren, A. DiNola, J.R. Haak, Molecular dynamics with coupling to an external bath, J. Chem. Phys. 81 (1984) 3684–3690.
[36] J.-P. Ryckaert, G. Ciccotti, H.J.C. Berendsen, Numerical integration of the Cartesian equations of motion of a system with constraints: molecular dynamics of *n*-alkanes, J. Comput. Phys. 23 (1977) 327–341.
[37] D.A. Case, T.E. Cheatham III, T. Darden, H. Gohlke, R. Luo, K.M. Merz Jr., A. Onufriev, C. Simmerling, B. Wang, R.J. Woods, The Amber biomolecular simulation programs, J. Comput. Chem. 26 (2005) 1668–1688.
[38] H. Park, S. Lee, J. Suh, Structural and dynamical basis of broad substrate specificity, catalytic mechanism, and inhibition of cytochrome P450 3A4, J. Am. Chem. Soc. 127 (2005) 13634–13642.
[39] N. Tokuriki, D.S. Tawfik, Protein dynamism and evolvability, Science 324 (2009) 203–207.
[40] A. Gutierrez, T. Yoshimura, Y. Fuchikami, K. Soda1, N. Esaki, A mutant D-amino acid aminotransferase with broad substrate specificity, Protein Eng. 11 (1998) 53–58.
[41] H.M. Wilks, D.J. Halsall, T. Atkinson, W.N. Chia, A.R. Clarke, J.J. Holbrook, Designs for a broad substrate specificity keto acid dehydrogenase, Biochemistry 29 (1990) 8587–8591.